Modeling the Thermo-Physical Properties of the Solids Using the Measured Distribution of Temperature Within the System of Contacting Solids at Uniform Heating

Dr. Sergei Fomin,
Fabio Capovilla-Searle, Noah Chicoine, Kyle Hammer, Cody Morrin,
Nathan Rutherford, Scotty Tilton

October 10, 2023

Abstract

The laboratory set up for determining the thermo-physical properties of materials under uniform heating is investigated. It is possible to derive a system of partial differential equations that models the laboratory set up. From which a non-dimensional system of partial differential equations can be derived. Once this system of equations is solved analytically, it is possible to implement two methods that use experimental data and the analytic solution to find the thermo-physical properties of the material being studied. The efficacy and precision of these methods is investigated.

1 Introduction

The device of the laboratory set up for defining thermo-physical properties of different materials, which is based on the concept of heat transfer regime of the third kind, is described in detail in [1,2]. This device is based on the following concept of the heat transfer process. The specimen of the material to be examined, which has the shape of cylindrical slab with radius $r_0 = 15mm$ and thickness $L = 20mm$, is placed between two semi-infinite solid media (such that the length of each medium must be much greater than the depth of penetration of temperature perturbations) with well documented thermo-physical properties, and the periodic heating performed at one of the interfaces between the examined specimen and the confining solid medium. Fig. 1 depicts the principal scheme of 3 contacting solids where the process of conductive heat transfer takes place. In this figure: 1, 3 – are solids with well-known thermo-physical properties (sample solids), 2 – the solid specimen under examination, 4 – heating module, which secures the uniform heating along the interface between the solids 1 and 2.

Assuming that the side surface of this array of three contacting cylindrical solids is ideally insulated, then the heat transfer within these solids takes place in the x-direction. In addition, to obtain a simpler formulae, it is necessary to assume that solid 1 in Fig.1 is an ideal insulator of heat, that is, the thermal conductivity of it is negligibly small. In this case, we have a system of two contacting solids, 2 and 3.

Publications [1,2] examine a situation when the heat flux from the heater 4 is periodic, that is, can be described by a periodic function. This periodic function can be presented by its Fourier series, which represents the infinite sum of the constant components of the heat flux and its different harmonics. Instead, we will examine the situation when the heat flux is a real valued constant function.

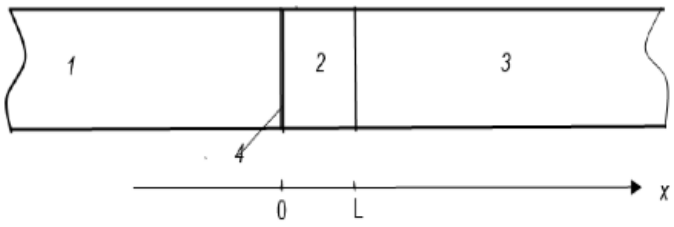

Figure 1: *The schematic sketch of three contacting solids (the cross-section of the cylindrical solids by the plane that contains the axis of symmetry of solids).*

Lastly, once the analytic solution of the problem with constant heat flux and the corresponding measurements of the temperatures in the solid are known, then multiple methods that determine the physical properties of the solid can be readily built. Therefore avoiding the procedure of expanding the analytic solutions into Fourier series.

Nomenclature

t_i	Temperature in the i-th solid
x	Spatial variable
τ	Time
L	The length of the solid under examination
a_i	Thermal diffusivity of the solid i
λ_i	Conductivity of the solid i
r_0	The radius of contacting solids
S	Area of the cross-section of contacting solids
t_0	Ambient temperature
q	Given heat flux from the heater
X	Non-dimensional distance
F_o	Non-dimensional time
Q	Non-dimensional Heat Flux
Λ	Non-dimensional Conductivity
A	Non-dimensional Thermal Diffusivity

2 Mathematical Model of the System of Heat Transfer

Heat conduction in solids 1 and 2 in the x-direction is described by the following equations and boundary conditions:

$$\frac{\partial(t_i - t_0)}{\partial \tau} = a_i \frac{\partial^2 (t_i - t_0)}{\partial x^2}, \quad \text{where} \quad i = 2, 3, \tag{2.1}$$

$$\tau = 0, \qquad t_i = t_0, \quad \text{for} \quad i = 2, 3, \tag{2.2}$$

$$x = 0, \qquad \lambda_2 \frac{\partial t_2}{\partial x} + q(\tau) = 0, \tag{2.3}$$

$$x = L, \qquad t_2 = t_3, \quad \text{and} \quad \lambda_2 \frac{\partial t_2}{\partial x} = \lambda_3 \frac{\partial t_3}{\partial x}, \tag{2.4}$$

$$x \to \infty, \qquad t_3 \to t_0, \tag{2.5}$$

where t_i - temperature in the i-th solid; x - spatial variable; τ - time; L - the length of the solid under examination; a_i, λ_i - thermal diffusivity and conductivity, respectively, of the solid i; r_0, S - the radius and area of the cross-section of contacting solids; t_0 - ambient temperature; q - given heat flux from the heater.

It is convenient to convert the variables in the system (2.1)-(2.5) into non-dimensional form by using the following relationships

$$\theta_i = \lambda_3 \frac{t_i - t_0}{L q_0^*}; \quad X = \frac{x}{L}; \quad F_o = \frac{\tau a_3}{L^2}; \quad Q = \frac{q}{q_0^*}; \quad \Lambda = \frac{\lambda_2}{\lambda_3}; \quad A = \frac{a_2}{a_3}; \tag{2.6}$$

where $q_0^* = N_0/S$ is the characteristic scale for the heat flux and N_0 is the power of the heater. As a result, the following system of non-dimensional equations is obtained

$$\frac{\partial \theta_i}{\partial F_o} = A_i \left[\frac{\partial^2 \theta_i}{\partial X^2} \right], \quad i = 2, 3 \qquad F_o > 0, \tag{2.7}$$

$$F_o = 0, \qquad \theta_i = 0, \quad i = 2, 3, \tag{2.8}$$

$$X = 0, \qquad \Lambda \frac{\partial \theta_2}{\partial X} + 1 = 0 \qquad F_o > 0, \tag{2.9}$$

$$X = 1, \qquad \theta_2 = \theta_3, \qquad \Lambda \frac{\partial \theta_2}{\partial X} = \frac{\partial \theta_3}{\partial X}, \qquad F_o > 0, \tag{2.10}$$

$$X \to \pm\infty, \qquad \theta_3 \to 0, \qquad F_o > 0. \tag{2.11}$$

In the above equations it is assumed that the heat flux is constant, i.e. $q_0^* = q$, $Q = 1$, and $A_2 = A$, $A_3 = 1$.

The system of equations (2.7)-(2.11) completely defines the temperature field in the system of contacting solids presented in Fig. 1.

3 Solution of the System of the Partial Differential Equations and the Analysis of the Solution

3.1 Derivation of the Major Formulae

Since the system of equations (2.7)-(2.11) is linear, it is sufficient to find the solution for when the heat flux is trivial, $Q = 1$, and then implement Duhamel's principle [3] to obtain the solution for when the heat flux is any constant function.

The solution to the system of equations (2.7)-(2.11) can be obtained through Laplace transforms [3] with respect to the variable F_o. Denoting

$$\Theta_i(s, R, X) = \int_0^\infty \theta_i(F_o, R, X) e^{-st} dF_o, \tag{3.1}$$

where s is the complex parameter, and applying the Laplace transform to the system (2.7)-(2.11), yields

$$\frac{s\Theta_i}{A_i} = \frac{\partial^2 \Theta_i}{\partial X^2}, \quad i = 2, 3, \tag{3.2}$$

$$X = 0, \quad \Lambda \frac{\partial \Theta_2}{\partial X} + \bar{Q}(s) = 0, \tag{3.3}$$

$$X = 1, \quad \Theta_2 = \Theta_3, \quad \Lambda \frac{\partial \bar{\Theta}_2}{\partial X} = \frac{\partial \Theta_3}{\partial X}, \tag{3.4}$$

$$X \to \pm\infty \quad \Theta_3 \to 0, \tag{3.5}$$

where $\bar{Q}(s) = 1/s$.

Solving equations (3.2)-(3.5) results in solutions to Θ_2 and Θ_3 that can be presented in the following form:

$$\Theta_2(X, s) = \frac{\bar{Q}\sqrt{A}}{\Lambda\sqrt{s}} \frac{g_+ e^{\sqrt{\frac{s}{A}}(1-X)} + g_- e^{-\sqrt{\frac{s}{A}}(1-X)}}{g_+ e^{\sqrt{\frac{s}{A}}} - g_- e^{-\sqrt{\frac{s}{A}}}}, \tag{3.6}$$

$$\Theta_3(X, s) = \frac{2\bar{Q}\sqrt{A}}{\Lambda\sqrt{s}} \frac{e^{-\sqrt{s}(X-1)}}{g_+ e^{\sqrt{\frac{s}{A}}} - g_- e^{-\sqrt{\frac{s}{A}}}}, \tag{3.7}$$

where $g_+ = 1 + \sqrt{A}/\Lambda$, $g_- = 1 - \sqrt{A}/\Lambda$.

Since the sensors that measure the temperature are located on solid 3, our major interest is to find the closed-form solution for θ_3. Since $\bar{Q}(s) = 1/s$, then (3.8) has the following form:

$$\Theta_3(X, s) = \frac{2\sqrt{A}}{\Lambda s\sqrt{s}} \frac{e^{-\sqrt{s}(X-1)}}{g_+ e^{\sqrt{\frac{s}{A}}} - g_- e^{-\sqrt{\frac{s}{A}}}}. \tag{3.8}$$

The latter formula can be converted to the form convenient for applying the inverse Laplace transform:

$$\Theta_3(X, s) = \frac{2\sqrt{A}}{\Lambda g_+ s^{3/2}} \sum_{k=0}^{\infty} \left(\frac{g_-}{g_+}\right)^k e^{-\sqrt{\frac{s}{A}}(\sqrt{A}(X-1)+2k+1)}. \tag{3.9}$$

Using the table of inverse Laplace transforms available in [3], according to which $L^{-1}\left\{\frac{e^{-\alpha\sqrt{s/A}}}{s\sqrt{s}}\right\} = 2\sqrt{F_o}\mathbf{i}\mathrm{erfc}(\frac{\alpha}{2\sqrt{AF_o}})$, the following formula for the temperature field in the solid 3 for the constant heat flux is:

$$\theta_3(X, F_o) = \frac{2\sqrt{AF_o}}{\Lambda g_+} \sum_{k=0}^{\infty} \left(\frac{g_-}{g_+}\right)^k \mathbf{i}\mathrm{erfc}\left(\frac{\sqrt{A}(X-1)+2k+1}{2\sqrt{AF_o}}\right), \tag{3.10}$$

where $\mathbf{i}\mathrm{erfc}(z) = \frac{1}{\sqrt{\pi}} e^{-z^2} - z\mathrm{erfc}(z)$, $\mathrm{erfc}(z) = 1 - \frac{2}{\sqrt{\pi}} \int_0^z e^{(-x^2)} dx$.

It should be noted that the quotient $g_-/g_+ < 1$ and the function $\mathbf{i}\mathrm{erfc}(z)$ is a rapidly decreasing function, so the series (3.10) rapidly converges.

3.2 Derivation of the Approximation of the Major Formulae

If the process for big values of time ($F_o \gg 1$) is of concern, then from formula (3.9) we can easily obtain the temperature field valid for big values of time. According to the theory of Laplace transforms, expression

Table 1: *Values of thermo-physical parameters.*

Parameter	r_0	L	λ_2	a_2	λ_3	a_3	q
Dimensions	M	M	$\frac{W}{MK}$	M^2/C	$\frac{W}{MK}$	M^2/C	$\frac{W}{M^2K}$
Typical Values	0.015	0.02	2.6	1.85×10^{-6}	16	4.4×10^{-6}	5

(3.9) can be presented for the case when $s \to 0$, and then the inverse Laplace transform can be applied. As a result, the following asymptotic temperature distribution is obtained:

$$\hat{\theta_3}(X, F_o) = 2\sqrt{\frac{F_o}{\pi}} e^{-\frac{(X-1)^2}{4F_o}} - \frac{1+\beta(X-1)}{\beta} \text{erfc}\left(\frac{X-1}{2\sqrt{F_o}}\right) + \frac{1}{\beta} e^{\beta(X-1)+\beta^2 F_o} \text{erfc}\left(\frac{X-1}{2\sqrt{F_o}} + \beta\sqrt{F_o}\right), \tag{3.11}$$

where $\beta = \frac{A}{\Lambda}, F_o \gg 1$. If $X = 1$, then (3.11) reduces to

$$\hat{\theta_3}(1, F_o) = 2\sqrt{\frac{F_o}{\pi}} - \frac{1}{\beta} + \frac{1}{\beta} e^{\beta^2 F_o} \textbf{i}\text{erfc}(\beta\sqrt{F_o}), \tag{3.12}$$

or to

$$\hat{\theta_3}(1, F_o) = 2\sqrt{\frac{Fo}{\pi}} - b + \frac{b^2}{\sqrt{\pi * F_o}} - \frac{b^4}{2F_o\sqrt{\pi * F_o}} + ..., \tag{3.13}$$

where $b = 1/\beta$.

Expressions (3.11)-(3.13) show that for large times, temperature in the prototype solid depends on only one non-dimensional parameter $b = \Lambda/A$. The obtained solutions can be validated by the numerical experiments described below.

3.3 Numerical Experiments

For the calculations of the numerical experiments, the values found in table 1 were used for the thermo-physical parameters.

A numerical inverse Laplace transform algorithm can be applied to Θ_3 in order to validate θ_3. Utilizing the `FT[`F, t, M`]` algorithm written by Abate and Valkó [2] results in a difference between θ_3 and `FT[`$\Theta_3, t, 32$`]` in the magnitude of 10^{-12} for observable values of F_o. A description of the `FT[`F, t, M`]` algorithm is in appendix 5.1 of this paper.

In addition, comparing the asymptotic approximation $\hat{\theta_3}$ with θ_3 using the parameters from table 1 shows that two terms of the asymptotic approximation is sufficient for approximating θ_3 (relative difference < 0.01 at $F_o = 54$). Fig. 2 shows this comparison at $X = 1$.

4 Models of the Thermo-Physical Properties of the Solids

Given temperature readings at certain time intervals, $\varphi(F_o)$, it is possible to find the thermal diffusivity, A and conductivity, Λ, of both solids (thanks to $A = a_2/a_3$ and $\Lambda = \lambda_2/\lambda_3$, if the properties of solid 3 are known). For the purpose of testing the methods we used, we added variations to θ_3, implementing Mathematica's `RandomReal` function on an interval [-0.1, 0.1], using the parameters from table 1. We named this new function $\varphi(k)$. Figure 3 shows a plot of simulated temperature data with θ_3 at $X = 1$.

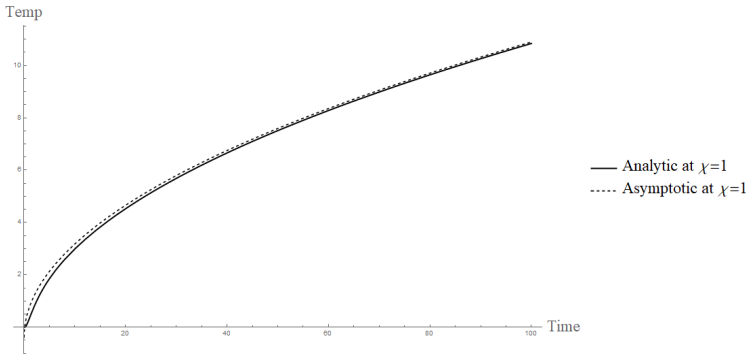

Figure 2: *Graph of θ_3 compared to the first two terms of $\hat{\theta_3}$ at $X = 1$.*

4.1 The Single J-Method

The single-J method is comprised of minimizing the square error function, J, of the analytic solution, θ_3, and the temperature readings, $\varphi(F_o)$, where thermal diffusivity and conductivity, Λ and A, are the variables of J:

$$J(A, \Lambda) = \sum_{k=0}^{F_{omax}} \left[\theta_3(X_{test}, k, A, \Lambda) - \varphi(k)\right]^2 . \tag{4.1}$$

X_{test} was the position at which the measurements were taken. The result of minimizing J is A^* and Λ^*, which are the thermo-physical values of the solids.

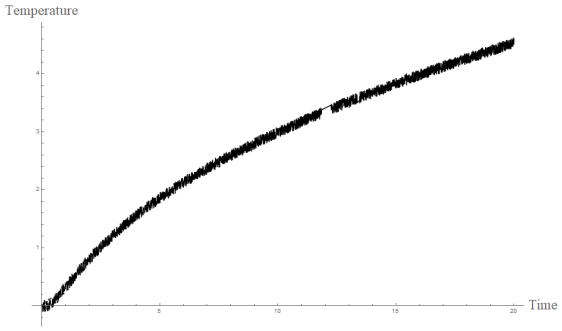

Figure 3: *Plot of $\varphi(F_o)$ at $X = 1$, using data from table 1.*

4.2 The Multi-J Method

The multi-J method is similar to the single J method, using two J functions instead. The first of the square error functions, J_1, is the square error function of the asymptomatic approximation of θ_3, $\hat{\theta_3}$, and $\varphi(F_o)$,

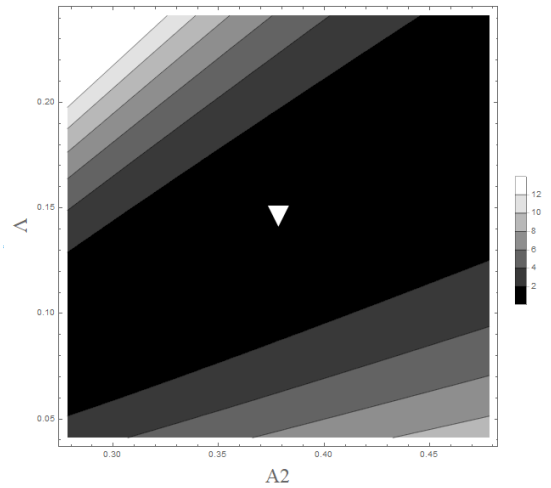

Figure 4: *Plot of $J(A, \Lambda)$ at $X_{test} = 1$ tested at integer time up to $F_{o_{max}} = 100$, to find parameters $A = 0.4204$, $\Lambda = 0.1625$. The minimum was found at $A^* = 0.3958$, $\Lambda^* = 0.1508$, denoted by the bottom of the triangle in the figure above.*

where the variable is b, since $b = A/\Lambda$:

$$J_1(b) = \sum_{k=k_{min}}^{N} \left[\hat{\theta}_3(X_{test}, F_o, b) - \varphi(k)\right]^2, \tag{4.2}$$

Note that a k_{min} value of 1000 is sufficient for the asymptotic approximation to be relatively close to the analytic solution (the relative difference is less than 10^{-2}). Once this function is minimized, the value of b^* is then used for the second square error function, J_2. J_2 is the square error function of θ_3 and $\varphi(F_o)$, where the variable is Λ:

$$J_2(\Lambda) = \sum_{k=0}^{M} \left[\theta_3(X_{test}, k, \frac{\Lambda}{b^*}, \Lambda) - \varphi(k)\right]^2. \tag{4.3}$$

Once Λ^* is found, then using the relationship with b, it is then possible to find A^*.

4.3 Comparison of the Different Methods

500 attempts to implement the single and multi-J methods were done with the same values. The results of these 500 attempts can be found in table 2. For the single J method the values were $X_{test} = 1$, $A = 0.4204$, $\Lambda = 0.1625$, and $F_{o_{max}} = 100$. For the multi-J method the values were $X_{test} = 1$, $b = 0.3864$, $A = 0.4204$, $\Lambda = 0.1625$, $N = 2000$, and $M = 100$. Both the single and multi methods shared the same $\varphi(F_o)$, but a new $\varphi(F_o)$ was generated for each attempt, and the minimum of the square error functions (4.1)-(4.3) was found using the Mathematica function `FindMinimum`. These attempts were run on a Macbook Pro 2015, with a 2.9 GHz Intel Core i5 processor, where the computation time was found using the Mathematica function `Timing`.

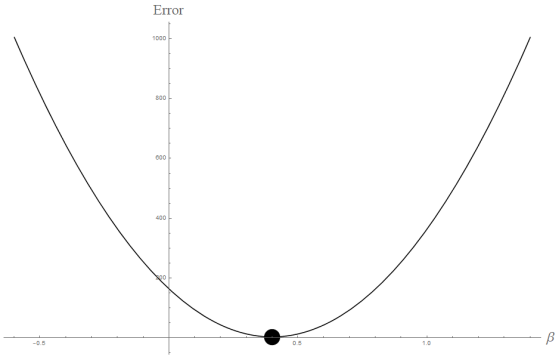

Figure 5: *Plot of $J_1(b)$ at $X_{test} = 1$ tested at integer time from $k_{min} = 1000$ to $N = 2000$, to find the parameter $b = 0.3865$. The minimum was found at $b^* = 0.4031$.*

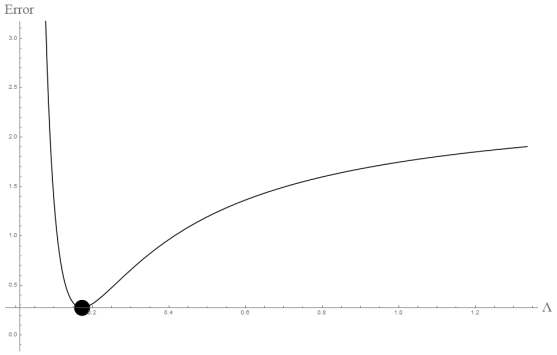

Figure 6: *Plot of $J_2(\Lambda)$ at $X_{test} = 1$ tested at integer time up to $M = 100$, to find the parameter $\Lambda = 0.1625$ (and subsequently $A = 0.4204$). The minimum was found at $\Lambda^* = 0.1774$ (and $A^* = 0.4402$).*

The single J method succeeded in finding the closest values to A and Λ, but, the computation time, while worse, was not unreasonable. Since the variance of the values was less than 10^{-3} in both cases, both methods were consistent. But if the aim is accuracy, the single J method is best. But if the aim is minimizing the computation time, the multi-J method is better.

Table 2: *The results of 500 attempts of both methods.*

	Mean A^*	Var. A^*	Mean Λ^*	Var. Λ^*	Mean Computation Time (s)
Single J	0.4241	0.000754	0.1646	0.000206	34.44
Multi-J	0.4553	0.000431	0.1830	0.0000752	3.96

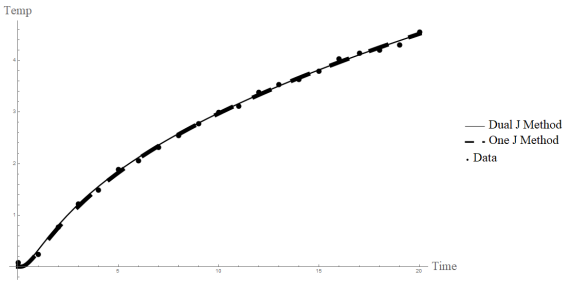

Figure 7: *A plot of how the analytic solution with the different parameters found in the single J method and the multi-J method inputted compares with the data collected for the first 20 data points.*

5 Conclusion

The methods that were developed to model the thermo-physical properties of the contacting solids are easy to implement and fast. The quantitative analysis of the methods demonstrated that both methods were very consistent. But, single-J method is more accurate while the multi-J method is faster. Furthermore, it is possible to extend the single-J method to account for different constant heat fluxes by using Duhammel's principle.

6 Appendix

6.1 FT Algorithm

To take the inverse Laplace transform of a function numerically, the `FT[F,t,M]` algorithm approximates the standard contour in the Bromwich integral,

$$f(t) = \frac{1}{2\pi i}\int_B e^{ts}F(s)ds, \tag{6.1}$$

with the function

$$\texttt{FT}[F,t,M] = \frac{r}{M}\left[\frac{1}{2}F(r)e^{rt} + \sum_{k=1}^{M-1}\mathrm{Re}[e^{t\cdot s(\theta_k)}F(s(\theta_k))(1+i\sigma(\theta_k))]\right], \tag{6.2}$$

with the substitutions

$$r = \frac{2M}{5t}, \quad s(\theta_k) = r\theta(\cot\theta_k + i), \quad \sigma(\theta_k) = \theta_k + (\theta_k\cot\theta_k - 1)\cot\theta_k \quad \text{and} \quad \theta_k = \frac{k\pi}{M}. \tag{6.3}$$

`FT[`F,t,M`]` increases in precision and computation time as M increases. However, since the difference between θ_3 and `FT[`$\Theta_3,t,32$`]` is in the magnitude of 10^{-12}, then $M = 32$ is satisfactory for accurate results.

6.2 Applying Duhamel's Principle for the Complete Solution

The complete solution of θ_i when Q is not necessarily 1, is given by

$$\theta_i(X,F_o) = \int_0^{F_o} q(0,\tau)\frac{d}{dF_o}\sum_{n=0}^{\infty}\theta_{i_n}(X,F_o-\tau)d\tau, \tag{6.4}$$

thanks to Duhamel's principle. Since

$$\mathcal{L}\left\{\frac{d}{dF_o}\theta_i(X,F_o)\right\} = s\bar{\theta}_i(X,s) - \theta_i(X,0) = s\bar{\theta}_i(X,s), \tag{6.5}$$

thanks to the boundary condition (2.8). Then, since the complete solution is a convolution, it commutes; so

$$\theta_i(X,F_o) = \int_0^{F_o} q(0,F_o-\tau)\frac{d}{dF_o}\sum_{n=0}^{\infty}\theta_{i_n}(X,F_o)d\tau. \tag{6.6}$$

6.2.1 The Complete Analytical Solution

The complete analytical solution for any constant Q, is given by

$$\begin{aligned}\theta_2(X,F_o) = \int_0^{F_o} q(0,F_o-\tau)\sum_{n=0}^{\infty}\Bigg[&\left(\frac{\sqrt{A}}{\sqrt{\pi}\Lambda\left(1+\frac{\Lambda}{\sqrt{A}}\right)}\right)\left(\sqrt{\frac{1}{A\tau}}\right)\left(\frac{-1+\frac{\Lambda}{\sqrt{A}}}{1+\frac{\Lambda}{\sqrt{A}}}\right)^n\\ &*\left(e^{\frac{2+4n+4n^2-2X+X^2}{2A\tau}}\right)\\ &*\left(\sqrt{A}\left(e^{\frac{(-2+2n+X)^2}{4A\tau}}-e^{\frac{(2n+X)^2}{4A\tau}}\right)+\Lambda\left(e^{\frac{(-2-2n+X)^2}{4A\tau}}+e^{\frac{(2n+X)^2}{4A\tau}}\right)\right)\Bigg]d\tau,\end{aligned} \tag{6.7}$$

$$\begin{aligned}\theta_3(X,F_o) = \int_0^{F_o} q(0,F_o-\tau)\sum_{n=0}^{\infty}\Bigg[&\left(\frac{2}{\sqrt{\pi}\left(1+\frac{\Lambda}{\sqrt{A}}\right)}\right)\left(\sqrt{\frac{1}{\tau}}\right)\left(\frac{-1+\frac{\Lambda}{\sqrt{A}}}{1+\frac{\Lambda}{\sqrt{A}}}\right)^n\\ &*\left(e^{-\frac{(1+2n+\sqrt{A}(-1+X))^2}{4A\tau}}\right)\Bigg]d\tau.\end{aligned} \tag{6.8}$$

References

[1] Abate J, Valkó PP. 2003. Numerical Inversion of Laplace Transform with Multiple Precision Using the Complex Domain. Wolfram Library Archive. library.wolfram.com/infocenter/MathSource/5026/.

[2] Abate J, Valkó PP. 2004. Multi-Precision Laplace transform inversion. Int. J. Numer. Meth. Engng. 60:979–993.

[3] Korn, G. A., & Korn, T. M. (2000). Mathematical handbook for scientists and engineers: Definitions, theorems, and formulas for reference and review (2nd ed.). Mineola: N.Y.